Steric Bulk-Dependent Photoresponse of Sulfonamide Azobenzene Ligand in Arene Ruthenium(II) Complexes

Jonathan Long, Pascal Retailleau, Juan Xie, Nicolas Bogliotti

doi.org/10.1002/hlca.202300190

RESEARCH ARTICLE

HELVETICA chimica acta

Steric Bulk-Dependent Photoresponse of Sulfonamide Azobenzene Ligand in Arene Ruthenium(II) Complexes

Jonathan Long,[a] Pascal Retailleau,[b] Juan Xie,[a] and Nicolas Bogliotti*[a]

[a] Université Paris-Saclay, ENS Paris-Saclay, CNRS, Photophysique et Photochimie Supramoléculaires et Macromoléculaires
91190, Gif-sur-Yvette, France, e-mail: nicolas.bogliotti@ens-paris-saclay.fr
[b] Université Paris-Saclay, CNRS, Institut de Chimie des Substances Naturelles, UPR 2301
91198, Gif-sur-Yvette, France

Dedicated to Prof. *Andrea Vasella* on the occasion of his 80th birthday

A series of sulfonamide azobenzenes bearing alkyl substituents of increasing steric bulk at the position *ortho* to the N=N bond and their corresponding chloro(hexamethylbenzene)ruthenium(II) complexes were synthesized. The latter bearing mono-substituted ligands exhibited an exocyclic azo bond under the *E* configuration, and underwent reversible *E*→*Z* photoisomerization upon irradiation with visible light, followed by thermal *Z*→*E* back isomerization upon resting in the dark at 20 °C. In contrast, the corresponding 2,6-dimethyl substituted azobenzene complex, while also exhibiting an exocyclic azo bond, was isolated as the *Z*-isomer and underwent uncommon solvent dependent irreversible photodissociation of azobenzene ligand upon visible light irradiation. Valuable insights into the photophysical and structural properties of these complexes were gained by combination of computational and X-ray diffraction studies.

Keywords: sulfonamide azobenzene, arene ruthenium, photoisomerization, TD-DFT, X-ray diffraction.

Introduction

Metal complexes bearing photochromic ligands, that can reversibly change between two different states in response to light, have attracted growing research interest recently due to the possible tuning of their structure and properties using a non-invasive stimulus. The potential applications of these molecular systems cover a variety of fields, such as controlling optical, redox and magnetic properties, self-association in both solution and solid state, biological activity and chemical reactivity, and notably catalytic behavior.[1–6] Among this class of photoresponsive molecules, ligands derived from azobenzene[4,7–15] and to a lesser extent aromatic imines,[16] play a special role because the N=N (or C=N) bond can function not only as the photoisomerizing unit, but also as the coordinating site. Consequently, these complexes undergo strong geometry modification in the vicinity of the metal center, which is likely to modulate molecular properties to a large extent. Our previous investigations focused on sulfonamide azobenzene ruthenium(II) arene complexes of type *E*-**A** (L=Cl, *Scheme 1*), revealing that modifcation of the arene ligand,[17] the sulfonamide moiety (by varying the X group),[17] and the phenyl ring (by varying the nature and position of the Y substituent),[17,18] primarily affected the rate of thermal back-isomerization from the isomer *Z*-**A** (obtained upon light irradiation) to the thermodynamically stable *E*-**A** form. By contrast, the replacement of the chlorido ligand with phosphine ligands (L=PPh_3, P(*p*-Tol)$_3$ and PBu_3) had a more profound impact since only the cationic complexes of the type *Z*-$\mathbf{A}^+$ were obtained, and they underwent phosphine ligand

Supporting information for this article is available on the WWW under https://doi.org/10.1002/hlca.202300190

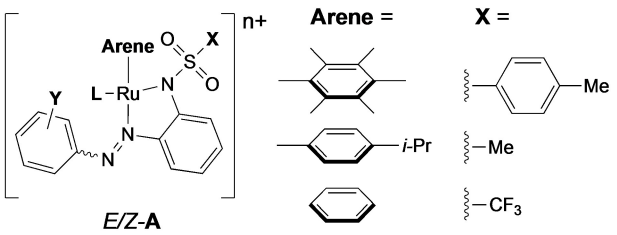

Y = 2-OMe, 4-OMe, 3-Br, 4-Br, 4-F, 2,6-diF
L = Cl, PPh_3, P(*p*-Tol)$_3$, PBu_3

Scheme 1. General structure of the previously synthesized photoresponsive sulfonamide azobenzene ruthenium(II) complexes (n = 0 for L=Cl; n = 1 for PPh_3, P(*p*-Tol)$_3$ and PBu_3).[17–19]

(L=PPh_3) photorelease upon light irradiation.[19] This uncommon behavior was advantageously exploited for the photoinitiation of catalytic aza-Morita–Baylis–Billman reaction[19] and Sonogashira cross-couplings.[20]

These results prompted us to investigate more systematically the influence of alkyl substituents with different steric bulk at the *ortho* position to the N=N bond on the structural and photoisomerization behavior of both sulfonamide azobenzene proligands **B** and their corresponding arene-Ru(II) complexes **C** (*Scheme 2*).

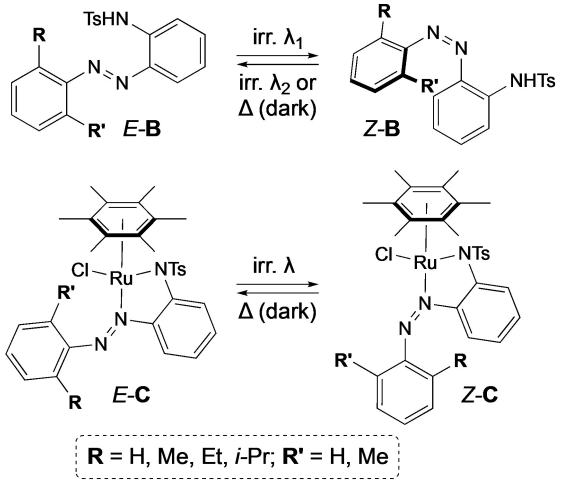

Scheme 2. Structure overview and expected photoisomerization behavior of the *o*-tosylamide azobenzene proligands and their corresponding arene Ru(II) complexes studied herein.

Results and Discussion

Synthesis

Sulfonamide azobenzene proligands **3**[17]–**7** were synthesized via an established route starting from *o*-phenylenediamine **1** (*Scheme 3*). Conversion to the nitroso **2**[17] was followed by reaction with several anilines of type **D** using standard Mill's conditions (acetic acid in refluxing toluene) to afford the desired azobenzene derivatives **3**[17]–**7** in 60–90% yield. Then, all the proligands obtained were reacted under identical conditions with 0.5 equivalent of dichloro(hexamethylbenzene)ruthenium(II) dimer [Ru(hmbz)Cl_2]$_2$ in the presence of Et_3N in MeOH at room temperature, following our well-established procedure (*Scheme 4*).[17,18] The complex *E*-**8**,[17] previously reported, was obtained from the unsubstituted (R/R' = H/H) proligand *E*-**3**, while mono-substituted sulfonamide azobenzenes *E*-**4**–**6** bearing alkyl groups of increasing steric bulk (Me, Et, *i*-Pr) led to similar results with isolation of complexes *E*-**9**–**11**, confirmed unambiguously by X-ray diffraction analysis (for *E*-**9**) and similarities observed in their photophysical behavior

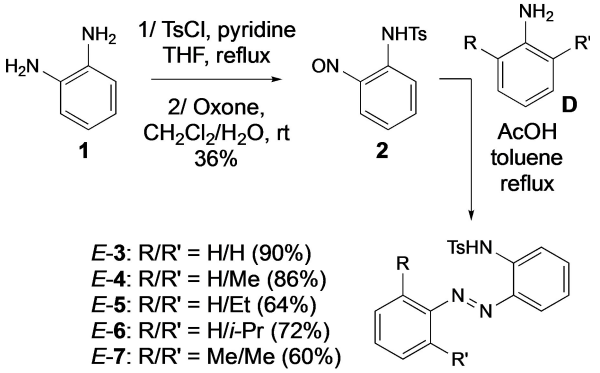

Scheme 3. Synthesis of *o*-tosylamide azobenzenes **3**–**7**.

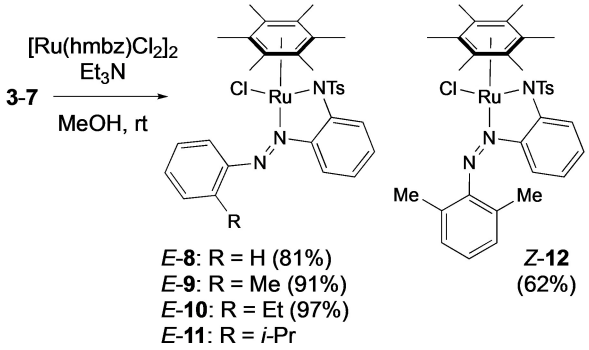

Scheme 4. Synthesis of *o*-tosylamide azobenzene arene Ru(II) complexes *E*-**8**-**11** and *Z*-**12**.

(see below). Yields for *E*-**9**–**10** spanned from 81% to 97%, while that of *E*-**11** could not be precisely determined due to some trace amounts of triethylammonium salt remaining after the workup procedure, which however did not affect the photophysical behavior (see below).

To our surprise, the reaction of *ortho* dimethyl sulfonamide azobenzene *E*-**7** under otherwise identical conditions as those previously used for other proligands **3**–**6**, led to the *Z*-configured complex **12** (whose structure was confirmed by X-ray diffraction studies, see below) that was isolated in a 62% yield, thereby evidencing the effect of steric bulk of substituent R and R′ on the geometry of the resulting Ru(II) complexes.

Photoisomerization Studies of the Tosylamide Azobenzene Proligands and their Arene Ru(II) Complexes

The UV-vis absorption spectrum of solutions of tosylamide azobenzenes **3**–**7** in CH_2Cl_2 was recorded. The observed patterns are herein discussed in detail for compound **4**, but appeared as quasi-identical for all compounds (*Figure 1a/b* and *Figures S1*–*S5*). Compound *E*-**4** prominently exhibits a strong absorption band with a maximum at 335 nm, a shoulder peak at 380 nm and a tail ranging approximately from 440 nm to 530 nm (*Figure 1a*). Upon irradiation at 334 nm, the intensity of the band gradually decreases while the maximum shifts to 319 nm with a shoulder observed at 370 nm. Concomitantly, a weaker broad band appears around 453 nm, and two isosbestic points are observed at 293 and 437 nm. Taken together, these features evidence *E*→*Z* photoisomerization of the azobenzene core, which is consistent with our previous reports (*Scheme 2*).[17,18] Upon resting in the dark at 20 °C, the solutions display absorption spectra that gradually evolve back toward the initial state, in agreement with thermal *Z*→*E* isomerization.

Monitoring the changes in absorbance over time using exponential fitting based on a first-order kinetic model enabled determination of the half-life ($t_{1/2}$) of *Z* isomer in azobenzene derivatives **3**–**7** (*Table 1* and *Figures S1*–*S5*).

Considering the series ranging from unsubstituted **3** (R, R′ = H) to monosubstituted derivatives **4**–**6** (R = H; R′ = Me, Et, *i*-Pr), it appeared that $t_{1/2}$ steadily decreases with an increase in steric bulk, with values ranging from 621 min to 249 min. By contrast, the rate of thermal *Z*→*E* isomerization rate of 2,6-dimethyl tosyla-

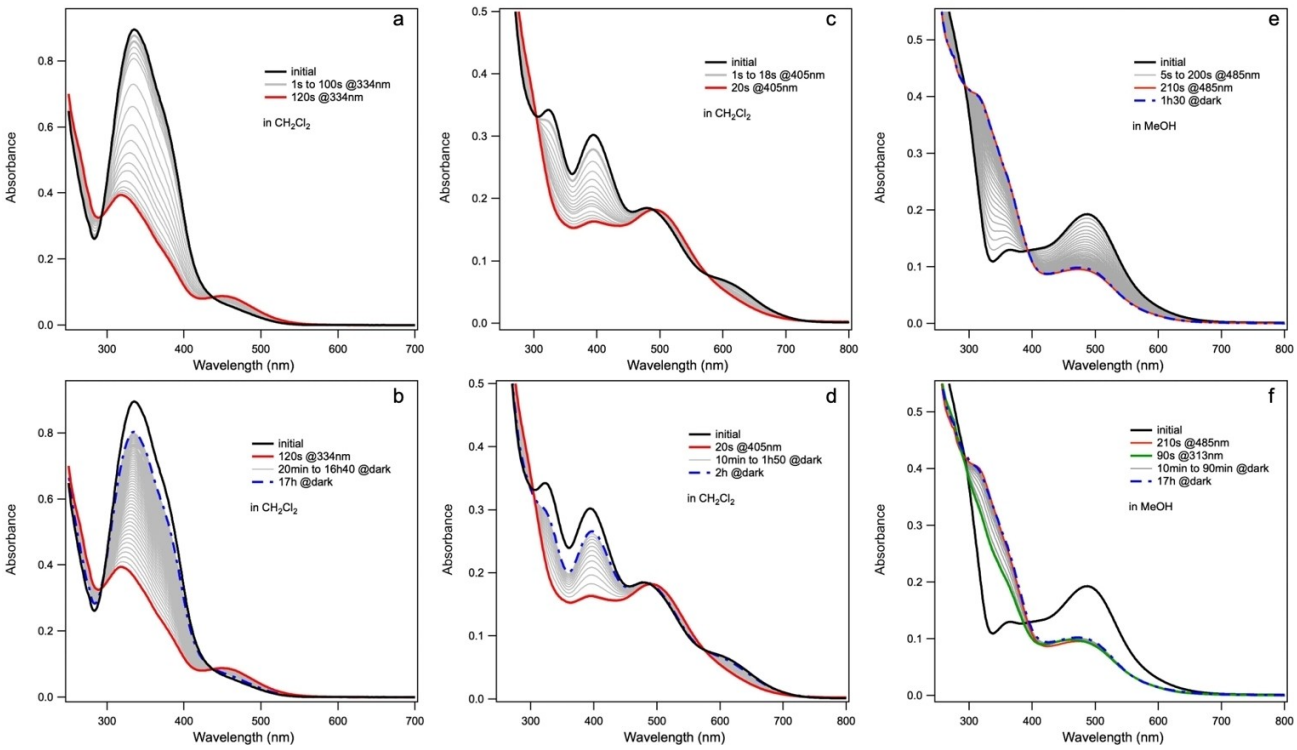

Figure 1. Absorption spectrum and its evolution upon irradiation followed by rest in the dark at 20 °C for *E*-**4** in CH_2Cl_2 (a/b), *E*-**9** in CH_2Cl_2 (c/d) and *Z*-**12** in MeOH (e/f). Irradiation wavelengths were 334, 405 and 485/313 nm for *E*-**4**, *E*-**9** and *Z*-**12**, respectively.

Table 1. Half-lives ($t_{1/2}$ in min) of the *Z* Isomers of proligands **3**–**7** and complexes **8**–**11** at 20 °C in CH_2Cl_2.

3	4	5	6	7	8	9	10	11
621	416	272	249	3526	22	62	46	63

mide azobenzene **7** was increased significantly to 3526 min, which supports the recent disclosure of the subtle influence of azobenzene structure and substitution pattern on its mechanism and the rate of thermal *Z*→*E* back-isomerization.[21,22]

The absorption spectrum of all *E*-configured complexes **8**–**11** showed great similarities (*Figure 1c/d* and *Figures S6*–*S9*). As an illustration, a solution of complex *E*-**9** in CH_2Cl_2 displayed two intense bands centered at 322 and 394 nm, as well as a less intense and broader one at 480 nm and a shoulder peak around 610 nm (*Figure 1c*). A significant spectral evolution was observed upon irradiation at 405 nm, with the disappearance of the bands at 322 nm and above 600 nm, and a drastic reduction of the intensity of the band at 394 nm. Meanwhile the intensity of the broad band remained constant and shifted to *ca.* 491 nm. The thermal *Z*→*E* back reaction occurred spontaneously in the dark at 20 °C as revealed by the gradual reversion of absorption spectra that revert to their initial state (*Figure 1d*). The calculated $t_{1/2}$ for the complexes *Z*-**8**–**11** ranged from 22 to 63 min, which was significantly lower compared to their corresponding proligands *Z*-**3**–**6**, and comparable to that of related structurally similar complexes previously reported.[17,18] The 2,6-dimethyl-substituted complex *Z*-**12** exhibited a singular behavior. Its UV-vis absorption spectra recorded in MeOH (*Figure 1e*) and CH_2Cl_2 (*Figure S10*) are quasi-identical and resemble those obtained for the *Z*-enriched mixtures upon irradiation of *E*-**8**–**11**. They exhibit a broad band centered around 494 nm and a weaker maximum intensity band at 363 nm. However, the behavior upon irradiation was highly dependent on the nature of the solvent. Indeed, no significant evolution could be observed by UV-vis spectroscopy upon irradiation at 485 nm of a solution of *Z*-**12** in CH_2Cl_2 (*Figure S10*). Conversely, using MeOH as the solvent resulted in a steady decrease of intensity of the band at 484 nm (associated with a slight blue-shift), upon irradiation at 485 nm, while overall absorption increased in the 300–400 nm range, with the emergence of a shoulder peak around 315 nm. Two isosbestic points were observed at 293 and 393 nm, strongly supporting a clean step-by-step conversion of *Z*-**12** into a single product. An intriguing feature was that, unlike other azobenzene proligands and complexes discussed above, no spectral evolution could be observed upon letting the system rest in the dark at 20 °C. Furthermore, irradiation at 313 nm resulted in the gradual decrease in absorbance in the 300–400 nm region; while the spectrum fully recovered its initial shape after resting in the dark at 20 °C for 17h. The photochemical reaction was carefully monitored by TLC after irradiation at 485 nm, and subsequent ^{1}H-NMR analysis showed the formation of tosylamide azobenzene *E*-**7**. This process was observed in a manner similar to that described by Phapale and Das[23] in benzimidazole arene-Ru(II) complexes (*Scheme 5*). While the fate of the chloro-arene-Ru component could not be elucidated, our observations are consistent with the fact that the system remains unchanged when left in the dark. Additionally, irradiation at 313 nm induces *E*→*Z* photoisomerization of **7**, followed by thermal *Z*→*E* back isomerization in the dark at 20 °C. The nature of the solvent played a critical role. Protic MeOH aids in ligand dissociation by providing a hydrogen atom to displace the ligand from the complex. This shift in equilibrium leads to the presence of neutral species *E*-**7**. Conversely, in aprotic CH_2Cl_2, dissociation of the *N*-deprotonated anionic form of the tosylamide azobenzene competes with its recombination to the metal center, resulting in no observable transformation overall.

Computational Studies

To understand the origin of UV-vis absorption bands and gain insight into the electronic transitions involved, geometry optimization was performed on both *E* and *Z* isomers of tosylamide azobenzenes **3**–**7** and complexes **8**–**11** (only *Z* isomer studied for **12**) by the density functional theory (DFT) method at the

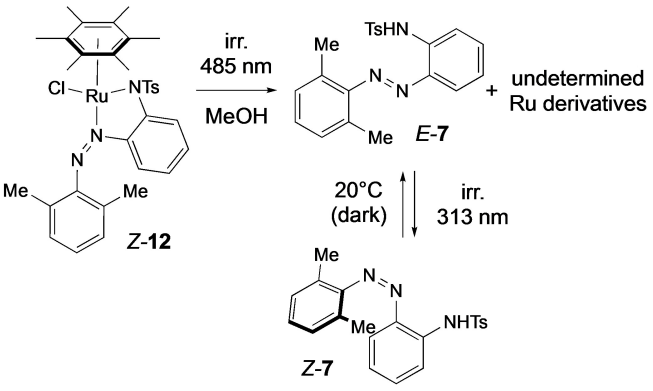

Scheme 5. Photochemical behavior of *Z*-**12**.

B3LYP/6–311G(d,p) level, using LANL2DZ basis set for Ru. The electronic transitions were calculated on these optimized structures by time-dependent DFT (TDDFT) at the PBE0/6–311+G(d,p) level (LANL2DZ for Ru). In most cases, the resulting excitation energies were found to originate from multiple transitions thereby precluding any clear qualitative visualization of the orbitals involved. We therefore generated natural transition orbitals (NTO) for the calculated excited states of interest.[24] The computational results obtained for tosylamide azobenzenes *E*/*Z*-**3**–**7** show high similarity and nicely match those obtained experimentally (*Table 2*, *Figure S11*, *Table S1* and *S2*). As an illustrative example, the strong UV-vis absorption band observed for *E*-**4** at 335 nm with a shoulder around 380 nm (*Figure 1a*), was found to originate from two transitions calculated at 334 and 384 nm, respectively, both showing a π→π* character from the aromatic rings to the N=N bond (*Table 2* and *Figure 2*). The long tail observed in the region 440–530 nm corresponds to a weaker transition calculated at 483 nm, showing n→π* character centered around the N=N bond. The bands observed at 317 nm (with shoulder at 370 nm) and 453 nm in the case of *Z*-enriched solutions of **4** (*Figure 1a*) can be understood by two π→π* transitions calculated at 308 and 354 nm, and a n→π* transition calculated at 502 nm (*Table 2* and *Figure 2*). These features are overall in agreement with what is commonly observed in azobenzene derivatives.[25]

Table 2. Characteristic UV-vis absorption wavelengths for the *E*/*Z* isomers of **3**–**7**.

	Exp.[a]	Calc.[b]		Exp.[a]	Calc.[b]
E-**3**	328	322 (π→π*)	*Z*-**3**	312	305 (π→π*)
	370[c]	385 (π→π*)		365[c]	356 (π→π*)
	425–530[d]	459[e] (n→π*)		453	498 (n→π*)
E-**4**	335	334 (π→π*)	*Z*-**4**	317	308 (π→π*)
	380[c]	384 (π→π*)		370[c]	354 (π→π*)
	440–530[d]	483 (n→π*)		453	502 (n→π*)
E-**5**	336	335 (π→π*)	*Z*-**5**	320	309 (π→π*)
	375[c]	383 (π→π*)		370[c]	353 (π→π*)
	425–530[d]	485 (n→π*)		455	502 (n→π*)
E-**6**	337	330 (π→π*)	*Z*-**6**	321	311 (π→π*)
	375[c]	379 (π→π*)		365[c]	355 (π→π*)
	420–530[d]	483 (n→π*)		462	508 (n→π*)
E-**7**	329	320 (π→π*)	*Z*-**7**	320	321 (π→π*)
	365[c]	377 (π→π*)		360[c]	348 (π→π*)
	415–560[d]	476 (n→π*)		460	505 (n→π*)

[a] Experimental values in nm in CH_2Cl_2 solution. [b] Calculated values in nm using the TD PBE0/6–311+G(d,p)//B3LYP/6–311G(d,p) method in gas phase and assignment determined from NTO analysis. [c] Shoulder. [d] Tail. [e] Shows oscillator strength close to 0.

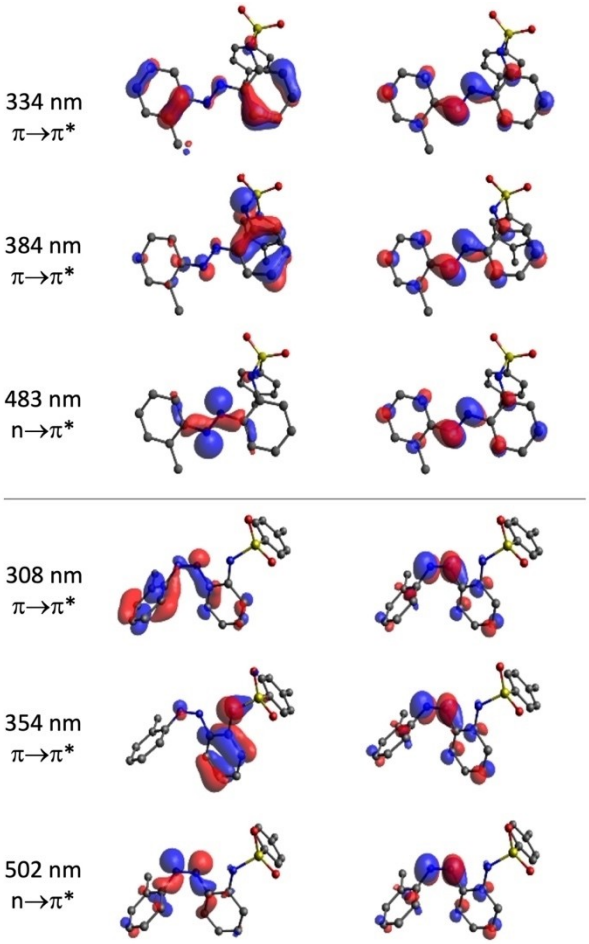

Figure 2. Natural transition orbitals pairs of *E*-**4** (top) and *Z*-**4** (bottom) from holes (left) to particles (right) for relevant electronic transitions calculated at the TD PBE0/6-311+G(d,p)//B3LYP/6-311G(d,p) level in gas phase.

The electronic transitions calculated for complexes **8**–**12** revealed high similarities between the *E* isomers on the one hand, and the *Z* isomers on the other hand, while proving in fair agreement with experimental results (*Table 3*, *Figure S12*, *Table S3* and *S4*). For example, the absorption bands exhibited by *E*-**9** at 322 and 394 nm, were found to correspond mostly to intraligand π→π* (calculated at 334 nm) and n→π* (calculated at 407 nm) transitions, respectively (*Table 3* and *Figure 3*). In contrast, the broader bands observed around 480 and 610 nm (calculated at 456 and 597 nm, respectively) were found to mostly exhibit a metal-to-ligand charge-transfer (MLCT) character from the Ru center to the π* orbital located at the N=N bond of the ligand. The absorption band observed at 395 nm for solutions enriched in *Z*-**9**, corresponded to a transition calculated at 370 nm showing mostly intra-

Table 3. Characteristic UV-vis absorption wavelengths for the *E*/*Z* isomers of complexes **8**–**12**.

	Exp.[a]	Calc.[b]		Exp.[a]	Calc.[b]
E-**8**	325	332 (π→π*)	*Z*-**8**	380	372 (MLCT)
	383	401 (n→π*)		492[d]	472 (MLCT)
	477	452 (MLCT)		–	504 (MLCT)
	610[c]	599 (MLCT)		–	529 (MLCT)
E-**9**	322	334 (π→π*)	*Z*-**9**	395	370 (π→π*)
	394	407 (n→π*)		491[d]	472 (MLCT)
	480	456 (MLCT)		–	506 (MLCT)
	610[c]	597 (MLCT)		–	530 (MLCT)
E-**10**	325[c]	334 (π→π*)	*Z*-**10**	413	370 (π→π*)
	403	408 (n→π*)		496[d]	472 (MLCT)
	483	456 (MLCT)		–	505 (MLCT)
	610[c]	596 (MLCT)		–	529 (MLCT)
E-**11**	325[c]	334 (π→π*)	*Z*-**11**	413	371 (MLCT)
	406	413 (n→π*)		496[d]	474 (MLCT)
	484	455 (MLCT)		–	506 (MLCT)
	610[c]	597 (MLCT)		–	531 (MLCT)
			Z-**12**	363	374 (MLCT)
				494[d]	468 (MLCT)
				–	489 (MLCT)
				–	576 (MLCT)

[a] Experimental values in nm in CH_2Cl_2 solution. [b] Calculated values in nm using the TD PBE0/6-311 + G(d,p){C,H,N,S,O,Cl}/LANL2DZ{Ru}//B3LYP/6-311G(d,p){C,H,N,S,O,Cl}/LANL2DZ{Ru} method in gas phase and assignment determined from NTO analysis. [c] Shoulder. [d] Broad.

Table 4. Selected experimental (XRD) and calculated (DFT) bond lengths (Å) and angles (°) for complexes *E*-**8**, *E*-**9**, and *Z*-**12**.

	E-**8**		*E*-**9**		*Z*-**12**	
	XRD	DFT[a]	XRD	DFT[a]	XRD	DFT[a]
Ru–N1	2.101(2)	2.126	2.100(3)	2.132	2.052(2)	2.082
Ru–N3	2.116(2)	2.104	2.121(2)	2.104	2.130(2)	2.108
N1 = N2	1.277(2)	1.263	1.270(4).	1.264	1.262(2)	1.261
N3-S1	1.631(14)	1.674	1.619(4)	1.674	1.613(2)	1.675
Ru-cent.[b]	1.710	1.837	1.715	1.837	1.687	1.815
N1-Ru–N3	77.4(6)	77.87	76.8(1)	77.90	76.29(5)	77.40
N1-Ru-Cl	94.5(4)	92.29	97.0(7)	92.13	85.96(4)	86.83
N3-Ru-Cl	88.7(4)	88.57	88.3(1)	88.27	92.61(4)	89.50
θ[c]	30.8	37.48	18.5 ± 2.5	36.72	69.9	68.38

[a] DFT at the B3LYP/6–311G(d,p){C,H,N,S,O,Cl}/LANL2DZ{Ru} method in gas phase. [b] cent. = centroid of hmbz ligand. [c] θ = angle between the planes of the two aromatic rings of the azobenzene ligand.

ligand π→π* character. In addition, according to computational studies, the very broad band with a maximum at 491 nm originates from several transitions (calculated at 472, 506 and 530 nm) showing pronounced MLCT character. The behavior was overall similar with *Z*-**12** in the sense that the four calculated transitions of interest (*i.e.* 374, 468, 489, 576 nm) corresponding to the bands observed at 363 and 495 nm, exhibit a marked MLCT character (*Table S5*).

Structural Studies by XRD

Crystals suitable for X-ray crystallographic analysis were obtained from CH_2Cl_2 solution of *E*-**8** as previously reported,[17] and by vapor diffusion of petroleum ether in an acetone solution of the complex *E*-**9**

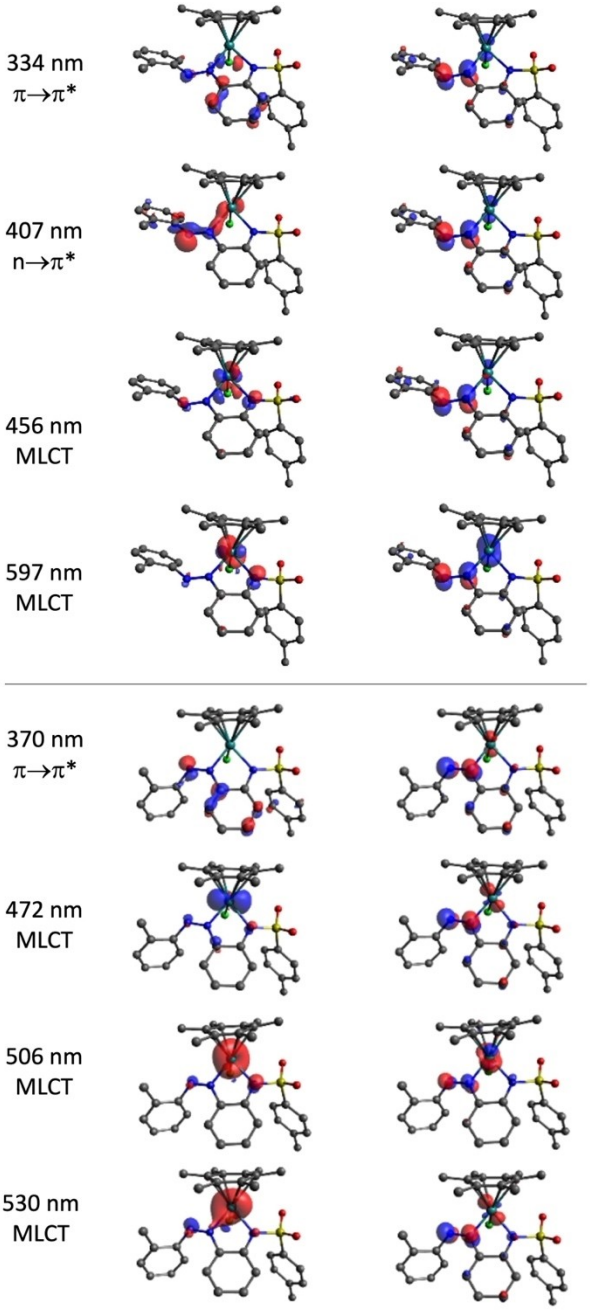

Figure 3. Natural transition orbitals pairs of *E*-**9** (top) and *Z*-**9** (bottom) from holes (left) to particles (right) for relevant electronic transitions calculated at the TD PBE0/6 311 + G(d,p)/LANL2DZ{Ru}//B3LYP/6-311G(d,p)/LANL2DZ{Ru} level in gas phase.

or *Z*-**12**.[1] Their respective crystal structures are shown in *Figure 4* and *Figure 5* and relevant geometric characteristics are reported in *Table 4*. Similar to *E*-**8**, *E*-**9** displays the classic feature of a "three-legged piano-stool" configuration at the ruthenium atom in a pseudo-octahedral geometry where the η^6-hexamethylbenzene (hmbz) ligand occupies one face and, most importantly, the tosylamide azobenzene moieties act as a bidentate *N*, *N* ligand forming a five-membered ring with an exocyclic N=N bond.

It should be emphasized that the presence of an *o*-tolyl group in *E*-**9** significantly reduces the distortion of the two aromatic rings of the azobenzene ligand as compared to *E*-**8**[17], as revealed by θ angle values between the two planes in the range of 16.1 – 20.1° and 30.8°, respectively. However, this effect is not observed in the case of *Z*-**12**, where the dimethylphenyl moiety is nearly perpendicular both to the second phenyl group (at 69.9°), and to the tosylate aromatic moiety (at 78.5°). The latter makes short contacts between H32 and Cl1 (2.841 Å) and O2 and H14 (2.378 Å), with a methyl group of the dimethylphenyl moiety directed towards the tosylate centroid (d = 3.904 Å); all these features contribute to a compact, folded sub-structure (*Figure 4*). Additionally, the ruthenium – arene centroid and Ru–N1 distances in *Z*-**12** (1.69 and 2.05 Å, respectively) are significantly

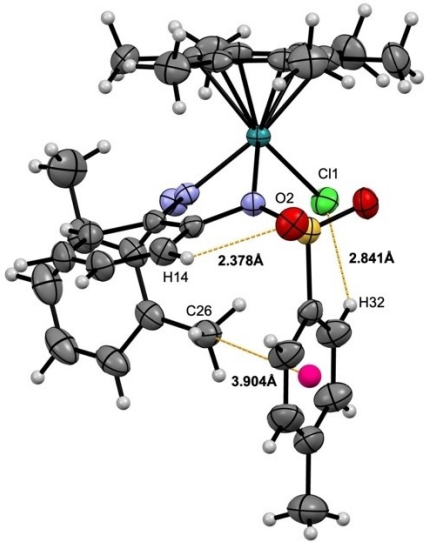

Figure 4. Details of the short contacts observed by XRD analysis in the folded substructure of *Z*-**12**.

[1]The presence of dichloromethane and diethyl ether molecules in the crystal structure of *E*-**9** originates from the workup procedure.

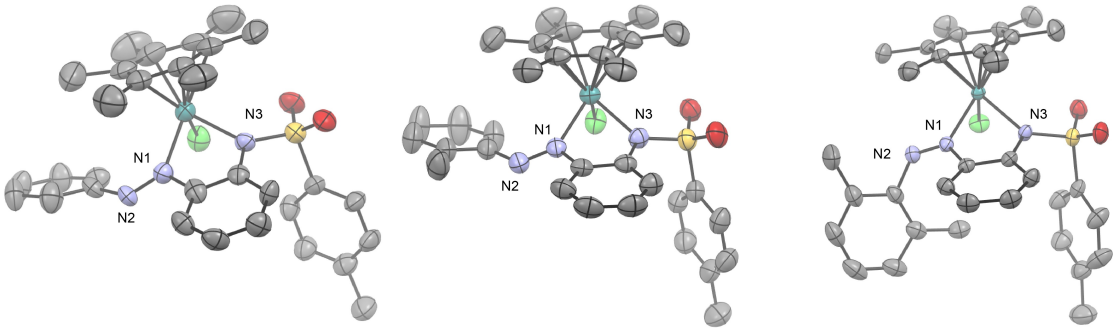

Figure 5. Ortep view of *E*-**8**, *E*-**9** and *Z*-**12**, from left to right. Displacement ellipsoids are drawn at the 50% of probability level. For clarity the hydrogen atoms are not shown.

reduced as compared to those found in *E*-**8** and E-**9** (1.71 and 2.10 Å, respectively for both complexes).

The structural parameters calculated by DFT for the three complexes are overall in good agreement with the experimental values, with the notable exception of the Ru-centroid distance which is overestimated (1.815–1.837 vs 1.687–1.715 Å) as previously observed for other hmbz-Ru(II) complexes.[26] In addition, while the θ angle value between the planes of the two aromatic rings of the azobenzene ligand is accurately predicted in *Z*-**12** (68.38 vs 69.9°), it differs significantly in the case of *E*-**8** (37.48 vs 30.8°) and *E*-**9** (36.72 vs 18.5°). This observation likely originates from the strong stacking interactions involving the aromatic groups of the azobenzene ligand that occur in the solid state (see below.)

The half-sandwich *E*-complexes display an azobenzene platform that is nearly parallel to the η^6-hmbz "seat", while the chlorine and SO_2 moiety of the tosylate group lie nearly parallel to the former plane. In contrast, the *o*-tolyl moiety acts as a crutch, being almost perpendicular to this sandwich-like complex (*Figure S14*). It results that both *E*-complexes crystallized in monoclinic unit cells, in which the molecules can stack, with the hmbz residing at the top of the azobenzene platform, while the tosylate group functions as a stacking guide, either along the ***a***-axis in columns parallel to the ***ac*** plane with rows propagating in the ***b*** direction anti-parallel, for the enantiomerically pure (R_{Ru})-*E*-**8**, or along the ***b***-axis in alternating racemic columns for *E*-**9** (*Figure 6*).[27] The molecular assemblies of the two complexes *E*-**8** and *E*-**9** display dissimilarities, ascribed to the presence of a methyl group in the *ortho* position of the azobenzene ligand in *E*-**9**. The $\pi-\pi$ stacking interactions delineate these differences through the variation of the centroid-to-centroid distance between the adjacent hmbz groups and *o*-tolyl groups. Indeed, the distance within the structure (R_{Ru})-*E*-**8** is 3.86 Å, whereas in the centrosymmetric structure *E*-**9**, it ranges from 3.64 to 4.46 Å due to the presence of two independently refined enantiomers in the asymmetric unit (*Figure 6*). If the *Z*-**12**

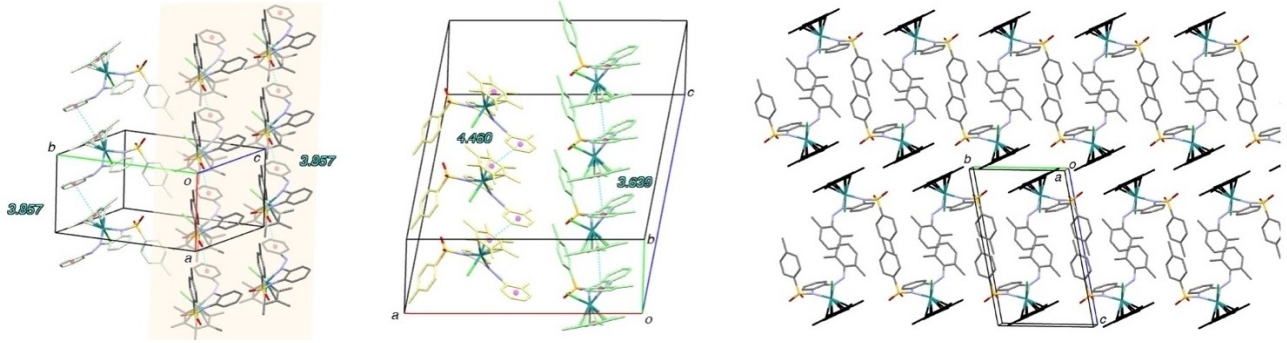

Figure 6. Views of the columnar arrangement of *E*-**8** (left; carbons in successive ***ac*** rows are of different grey colors) and *E*-**9** (middle; isomer R_{Ru}: carbons in pale yellow, isomer S_{Ru}: carbons in water green). View of the crystal packing of *Z*-**12** down the ***a*** axis (right), the hmbz rings are colored in black to highlight the bilayer arrangement

molecules are related by a center of inversion in a triclinic unit cell, they segregate the hmbz "seats" by positioning the legs of the stool, namely the dimethylphenyl ring of the azobenzene moiety and the tosylate ring, in between and nearly perpendicular to the stool platforms, which form bilayers of *c*/2 width and are oriented in parallel to the ***ab*** plane. In between, the tolyl rings are oriented in such a way to favor C–H···π interactions, which is in line with the fifth of the total contribution from the C···H/H···C contacts (*Figure 8* and *S23*).

Both monoclinic unit cells leave cavities (*E*-**8** and *E*-**9**), or channels (*E*-**9**) along the helicoidal two-fold rotation axis parallel to the crystallographic ***b*** axis. Crystallizing solvent molecules can enter these voids, contributing to packing cohesion (*Figure 7*). In *Z*-**12**, the hmbz groups are lying around the ***ab*** plane and, due to steric hindrance, they leave some voids, which are too small to be filled.

Intermolecular interactions in the Ru complexes were further investigated and visualized by Hirshfeld surfaces (HS), which have been mapped over a normalized contact distance, d_{norm}, which was defined in terms of d_i (resp. d_e), representing the distance of any surface point nearest to the internal (resp. exterior) atoms, and the van der Waals (vdW) radii of the atoms.[29,30] Molecular Hirshfeld surfaces calculations were performed using the Crystal Explorer package v.21.3.[31] All of the bond lengths to hydrogen were automatically modified to the standard neutron values (*e.g.* CH = 1.083 Å) in each input file. A color code is used to display normalized contact distance (d_{norm}): white for contacts around the vdW atomic radius separation ($d_{norm} = 0$), blue for longer contacts ($d_{norm} > 0$), and red for shorter contacts ($d_{norm} < 0$). A list of close interactions with shorter contact distances is given in *Table S7*, identified by the red spots of variable intensity on the HS for the three complexes (*Figure 8*). It is apparent that the complexes *E*-**8** and *E*-**9** do not display many red spots and the most intense ones (proportional to $\Delta|(d_{norm}-\Sigma_{rvdW})_{X\cdots Y}|$) are attributable to solvent molecules trapped in the crystal packing, particularly the dichloromethane, which forms short contacts via its hydrogen atoms with the oxygen atoms of the sulfonamide groups in both *E* complexes and also with the chlorine atom of one *E*-**9**. In both *E*-crystals, the contribution to the Hirshfeld surface is largely dominated by H···H interactions (almost 2/3 of the total interactions), followed by C–H···π interactions (one fifth of the total interactions) due to the orthogonally arranged aromatic rings (*Figure S21* and *S22*). Oxygen and chlorine atoms in the

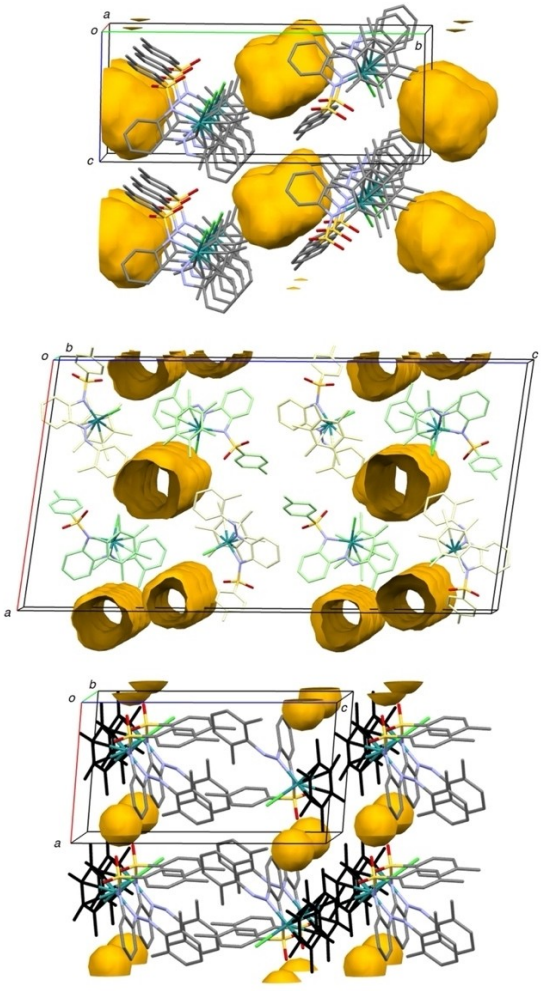

Figure 7. Part of the crystal structures of *E*-**8** (top), *E*-**9** (middle) and *Z*-**12** (bottom) showing voids or tunnels in which crystallizing solvent molecules are present (*E*-**8** and *E*-**9**) or absent (*Z*-**12**) using the Mercury software.[28] The probe radius for the voids is 1.2 Å.

complex are readily accessible to vicinal molecules present in the crystal packing and form unconventional H-bonds, spotted in red on the Hirshfeld surface. In comparison to the crystal structures of *E*-complexes, the red spots are more numerous on the HS for *Z*-**12** and imply less pairs of atoms, *i.e.* H/H, C/H, O/H, Cl/H and none of them from exogenous molecules (*Figure 8, Table S7* and *Figure S23*). The brightest spots are located at the top of the stool and involve contacts between a methyl hydrogen and a phenyl ring carbon from an adjacent hmbz within the two-hmbz layer. There, the crown of methyl groups acts as a barrier to prevent overlapping of the hmbz rings, unlike the columnar *E* crystal packings where π–π stacking between hmbz and the phenyl ring (*E*-**8**) and/or *o*-tolyl

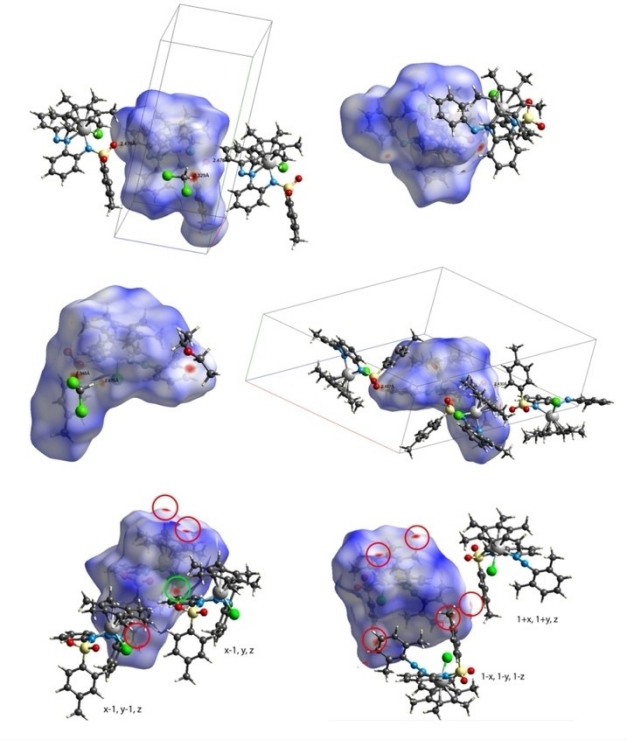

Figure 8. View of the HS mapped over d_{norm} for *E*-**8** over the range −0.2042 to +1.5188 a.u. (top), *E*-**9** over the range −0.1898 to +1.5206 a.u. (middle) and *Z*-**12** over the range −0.1452 to +1.7358 a. u. (bottom). Color-coded circles highlighting the short contacts refer to *Figure S23*.

ring (*E*-**9**) can take place (see shape index and curvedness HS in *Figures S24–S26*).

Conclusions

A series of sulfonamide azobenzene derivatives, which include varying steric bulk alkyl groups at the *ortho* position to the N=N bond were synthesized. These derivatives were then used as proligands in a reaction with dichloro(hexamethylbenzene)ruthenium(II) dimers. The resulting complexes resulting from monosubstituted azobenzenes were isolated as *E*-isomers that exhibit an exocyclic N=N bond. They underwent facile *E*→*Z* photoisomerization followed by spontaneous thermal back *Z*→*E* isomerization upon resting in the dark at 20 °C. In contrast, the dimethyl-substituted tosylamide azobenzene proligand exclusively formed the corresponding *Z*-isomer (still exhibiting exocyclic N=N bond). Upon irradiation in MeOH, this isomer underwent uncommon irreversible photodecoordination of the azobenzene ligand. The photophysical properties of both proligands and complexes were experimentally studied by UV-vis absorption and theoretically by TDDFT calculations. In-depth analysis of the crystal structure of three complexes evidenced the subtle influence of the ligand substitution pattern on molecular assembly and packing in the crystal state.

Experimental Section

General Information

Commercially available solvents and reagents were used without further purification. Reactions were monitored by Thin Layer Chromatography (TLC) using commercial TLC Silica gel 60 F_{254} with detection by UV light (254 nm or 365 nm). Column chromatography purification was performed on CombiFlash-Rf with UV-vis detection (two channels). NMR spectra were recorded using a JEOL ECS-400 or a Bruker AV500 spectrometer. Irradiation frequencies of ^{1}H and ^{13}C are respectively 399.78 MHz and 100.53 MHz or 500 MHz and 125 MHz. When specified, ^{13}C-NMR spectra of species were recorded using UDEFT sequence.[32] Chemical shifts are reported in delta (δ) units part per million (ppm) relative to the residual solvent signal or $Si(CH_3)_3$.[33,34] Coupling constants are reported in Hertz (Hz). The following abbreviations are used: s = singlet, d = doublet, t = triplet, q = quartet, sept. = septuplet, m = multiplet, br = broad. Melting points were measured with a Köfler bench previously calibrated. Infrared spectra were measured using a FTIR spectrometer from Thermo Electron Corporation with a Nexus model equipped with an ATR-Germanium module. Spectra were recorded using OMNI software. High-resolution mass spectra (HRMS) were performed on a Bruker maXis mass spectrometer by the "Fédération de Recherche" ICOA/CBM (FR2708) platform. Single crystals for X-Ray diffraction were obtained as described in experimental procedures and analyzed by the Structural Crystallography Platform of the Institut de Chimie des Substances Naturelles (CNRS, UPR2301, Université Paris-Saclay, Gif-sur-Yvette).

Deposition Numbers SACMIV (for *E*-**8**), 2271261 (for *E*-**9**), 2271262 (for *Z*-**12**) contain the supplementary crystallographic data for this paper. These data are provided free of charge by the joint Cambridge Crystallographic Data Centre and Fachinformationszentrum Karlsruhe Access Structures service.

Absorption spectra and irradiation experiments were performed in 1 cm path length quartz cells using

spectroscopic grade solvents. Absorption spectra were recorded on a Cary-100, Cary-4000 or Cary-5000 spectrophotometer from Agilent Technologies. Photochromic reactions were induced *in situ* by a continuous irradiation with Hg/Xe lamp (Hamamatsu, LC6 Lightningcure, 200 W) equipped with a narrow band interference filter of appropriate wavelength (Semrock FF01-335/7-25 for $\lambda_{irr} = 334$ nm, FF01-406/15-25 for $\lambda_{irr} = 405$ nm, FF01-485/20-25 for $\lambda_{irr} = 485$ nm). Stepwise irradiation of a compound in solution at the desired wavelength was performed until photostationary state (PSS) was reached, *i.e.* no further evolution of the spectrum could be observed.

Irradiance was measured using an Ophir photodiode (PD300-UV), and ranged between 5 to 30 mW.cm^{-2} at the wavelengths specified above. For half-life determination of *Z* isomers, a compound in solution was irradiated at the appropriate wavelength until PSS was reached and the solution was then allowed to stand protected from light at constant temperature (20 °C) while absorption spectra were recorded at regular time intervals. The kinetic constants of the thermal isomerization processes were extracted by exponential fitting of the absorbance at the appropriate wavelength, according to a first-order kinetic model. Molecular geometries were optimized by the DFT method using the B3LYP functional, the 6-311G(d,p) basis set and LANL2DZ for the ruthenium, as implemented in the Gaussian16 software package.[35] The absence of negative frequency was checked to confirm the obtention of an energy minimum. Excitation energies and oscillator strengths were calculated by the TDDFT method using PBE0 functional, the 6-311 + G(d,p) basis set and LANL2DZ for the ruthenium. When required, natural transition orbitals (NTO) analysis was performed on relevant transitions following an established method.[24] Molecular structures, orbitals and computed data were visualized and analyzed with Avogadro software.[36]

4-Methyl-*N*-(2-nitrosophenyl)benzenesulfonamide (2).[17] To a solution of *o*-phenylenediamine (2.00 g, 18.5 mmol) in THF (30 mL) were added pyridine (5.0 mL, 62 mmol, 3.0 eq.) and *p*-toluenesulfonyl chloride (3.43 g, 18.5 mmol, 1.0 eq.). After stirring under reflux for 40 min, the mixture was concentrated under reduced pressure. The residue was dissolved in CH_2Cl_2 (30 mL) and aq. HCl 0.1 M solution (30 mL) was added. Layers were separated and the aqueous layer was extracted with CH_2Cl_2 (*ca.* 2×20 mL), the organic layer was dried over $MgSO_4$, filtered and the solvent removed under reduced pressure to afford crude *N*-(2-aminophenyl)-4-methylbenzenesulfonamide[37] which was used for the next step without further purification. To a solution of this material (2.13 g, considered as 8.12 mmol) in CH_2Cl_2 (50 mL) was added dropwise a solution of Oxone® (5.89 g, 19.54 mmol, 2.4 eq.) in water (50 mL). After stirring vigorously at rt for 24h, the layers were separated. The aqueous layer was extracted with CH_2Cl_2 (*ca.* 2×50 mL), the combined organic layers were washed with brine, dried over $MgSO_4$, filtered and the solvent removed under reduced pressure. Purification by silica gel chromatography (petroleum ether/EtOAc: 7/3) afforded **2**[17] (808 mg, 2.92 mmol, 36% for 2 steps). Green solid. R_f 0.56 (petroleum ether/EtOAc: 7/3); ^{1}H-NMR (400 MHz, $(CD_3)_2CO$): 10.85 (brs, 1H), 7.97 (dd, $J = 7.5$, 2.0 Hz, 1H), 7.88 (d, $J = 8.0$ Hz, 2H), 7.80 (td, $J = 7.5$, 2.0 Hz, 1H), 7.36 (d, $J = 8.0$ Hz, 2H), 7.17 (td, $J = 7.5$, 1.0 Hz, 1H), 6.74 (dd, $J = 7.5$, 1.0 Hz, 1H), 2.37 (s, 3H). ^{13}C NMR (100 MHz, $(CD_3)_2CO$): 158.5, 145.5, 139.7, 139.5, 137.7, 130.8 (2C), 128.4 (2C), 124.3, 122.3, 114.0, 21.5.

General Procedure A for the Synthesis of o-Sulfonamide Azobenzenes **3–7**

To a solution of **2** in toluene were added aniline derivative (1.0 eq.) and acetic acid (4.0 eq.). After stirring under reflux (110 °C) for 24h, the mixture was concentrated under reduced pressure. The residue was dissolved in CH_2Cl_2 and a saturated aqueous solution of $NaHCO_3$ was added. Layers were separated and the aqueous layer was extracted with CH_2Cl_2. The combined organic layers were dried over $MgSO_4$, filtered and the solvent removed under reduced pressure. Purification by silica gel chromatography afforded the desired *o*-sulfonamide azobenzene.

Sulfonamide Azobenzene Proligand *E*-**4**, Synthesized according to general procedure A using **2** (100 mg, 0.360 mmol), *o*-toluidine (38 µL, 0.36 mmol) and acetic acid (82 µL, 1.5 mmol) in toluene (4.0 mL). Purification by silica gel chromatography (petroleum ether/EtOAc: 8/2) afforded **4** (114 mg, 0.29 mmol, 86% yield). Orange solid. M.p. 139 °C. R_f 0.64 (petroleum ether/EtOAc: 8/2). ^{1}H-NMR (400 MHz, $(CD_3)_2CO$): 10.13 (brs, 1H), 7.77–7.74 (m, 2H), 7.70 (d, $J = 8.5$ Hz, 2H), 7.63 (d, $J = 8.0$ Hz, 1H), 7.53–7.48 (m, 1H), 7.47–7.42 (m, 2H), 7.36–7.31 (m, 1H), 7.29–7.24 (m, 1H), 7.22 (d, $J = 8.0$ Hz, 2H), 2.70 (s, 3H), 2.27 (s, 3H). ^{13}C NMR (100 MHz, $(CD_3)_2CO$): 151.2, 144.9, 142.7, 139.3, 137.8, 135.8, 133.1, 132.7, 132.4, 130.5 (2C), 128.1 (2C), 127.5,

125.7, 122.9, 122.6, 116.5, 21.4, 18.0. IR (ATR): 3528, 3277, 2918, 1596, 1484, 1370, 1338, 1304, 1278, 1220, 1190, 1165, 1150, 1114, 1092, 1035, 1020, 946, 922, 903, 845, 817, 764, 756, 730, 708, 673, 661. UV/Vis (MeOH): 333 (15800). HR-ESI-MS: 366.1232 ($C_{20}H_{20}N_3O_2S$, $[M+H]^+$; calc. 366.1267).

Sulfonamide Azobenzene Proligand *E*-**5**. Synthesized according to general procedure A using **2** (100 mg, 0.360 mmol), 2-ethylaniline (45 μL, 0.36 mmol) and acetic acid (82 μL, 1.5 mmol) in toluene (4.0 mL). Purification by silica gel chromatography (petroleum ether/EtOAc: 9/1) afforded **5** (88 mg, 0.23 mmol, 64% yield). Orange solid. M.p. 90 °C. R_f 0.30 (petroleum ether/EtOAc: 9/1). ^{1}H-NMR (400 MHz, $(CD_3)_2CO$): 9.98 (brs, 1H), 7.78–7.68 (m, 4H), 7.64 (d, J = 8.0 Hz, 1H), 7.54–7.44 (m, 3H), 7.35 (td, J = 8.0, 1.5 Hz, 1H), 7.27 (td, J = 8.0, 1.5 Hz, 1H), 7.22 (d, J = 8.0 Hz, 2H), 3.14 (q, J = 8.0 Hz, 2H), 2.26 (s, 3H), 1.28 (t, J = 8.0 Hz, 3H). ^{13}C NMR (100 MHz, $(CD_3)_2CO$): 150.6, 145.3, 144.9, 142.9, 137.8, 136.2, 133.2, 133.0, 130.9, 130.5 (2C), 128.1 (2C), 127.6, 125.9, 123.0, 121.8, 116.6, 25.5, 21.4, 17.0. IR (ATR): 3272, 2968, 1595, 1478, 1444, 1425, 1373, 1337, 1298, 1278, 1221, 1188, 1167, 1148, 1110, 1090, 1040, 1018, 947, 923, 904, 870, 836, 813, 790, 768, 756, 729, 705, 694, 674, 663. HR-ESI-MS: 380.1388 ($C_{21}H_{22}N_3O_2S$, $[M+H]^+$; calc. 380.1429).

Sulfonamide Azobenzene Proligand *E*-**6**. Synthesized according to general procedure A using **2** (200 mg, 0.720 mmol), 2-isopropylaniline (100 μL, 0.720 mmol) and acetic acid (165 μL, 2.89 mmol) in toluene (7.5 mL). Purification by silica gel chromatography (petroleum ether/EtOAc: 9/1) afforded **6** (203 mg, 0.516 mmol, 72% yield). Orange solid. M.p. 95 °C. R_f 0.66 (petroleum ether/EtOAc: 9/1). ^{1}H-NMR (400 MHz, $(CD_3)_2CO$): 9.86 (brs, 1H), 7.77 (dd, J = 8.5, 1.5 Hz, 1H), 7.73–7.68 (m, 3H), 7.61 (d, J = 8.5 Hz, 1H), 7.56–7.49 (m, 3H), 7.36–7.31 (m, 1H), 7.27–7.20 (m, 3H), 4.05 (sept., J = 7.0 Hz, 1H), 2.26 (s, 3H), 1.33 (d, J = 7.0 Hz, 6H). ^{13}C NMR (100 MHz, $(CD_3)_2CO$): 150.1, 149.2, 144.9, 143.1, 137.9, 136.5, 133.3, 133.1, 130.6 (2C), 128.2 (2C), 127.4 (2C), 125.9, 123.1, 121.2, 116.6, 28.6, 24.2 (2C), 21.5. IR (ATR): 3265, 2960, 1596, 1478, 1456, 1382, 1332, 1305, 1273, 1222, 1185, 1165, 1152, 1092, 1038, 1030, 950, 908, 837, 813, 770, 749, 706, 693, 661. HR-ESI-MS: 394.1545 ($C_{22}H_{24}N_3O_2S$, $[M+H]^+$; calc. 394.1586).

Sulfonamide Azobenzene Proligand *E*-**7**. Synthesized according to general procedure A using **2** (200 mg, 0.720 mmol), 2,6-dimethylaniline (88 μL, 0.72 mmol) and acetic acid (165 μL, 2.89 mmol) in toluene (7.5 mL). Purification by silica gel chromatography (petroleum ether/EtOAc: 9/1) afforded **7** (163 mg, 0.430 mmol, 60% yield). Orange solid. M.p. 90 °C. R_f 0.33 (petroleum ether/EtOAc: 9/1). ^{1}H-NMR (400 MHz, $(CD_3)_2CO$): 9.95 (brs, 1H), 7.80 (dd, J = 8.5, 1.5 Hz, 1H), 7.77–7.71 (m, 3H), 7.52 (td, J = 8.5, 1.5 Hz, 1H), 7.31 (d, J = 8.0 Hz, 2H), 7.27–7.19 (m, 4H), 2.34 (s, 3H), 2.33 (s, 6H); ^{13}C NMR (100 MHz, $(CD_3)_2CO$): 151.3, 145.1 (2C), 141.7, 137.8, 135.8, 133.5, 132.4, 130.7 (2C), 130.4 (2C), 130.2, 129.0, 128.1 (2C), 125.2, 120.9, 21.4, 19.7 (2C). IR (ATR): 3315, 3039, 2919, 1595, 1479, 1468, 1376, 1336, 1309, 1286, 1219, 1188, 1164, 1147, 1090, 1036, 943, 918, 883, 842, 831, 816, 764, 754, 742, 723, 704, 661. UV/Vis (MeOH): 325 (10600). HR-ESI-MS: 380.1425 ($C_{21}H_{22}N_3O_2S$, $[M+H]^+$; calc. 380.1388).

General Procedure B for the Synthesis of Ruthenium Complexes **8–12**

To a solution of *o*-sulfonamide azobenzene **3**–**7** in MeOH were added NEt_3 (2.0 eq.) and $[Ru(hmbz)Cl_2]_2$ (0.5 eq.). The mixture was stirred overnight. The work-up procedure for each complex is detailed below.

Ru(II) Complex *E*-**9**. Synthesized according to general procedure B using **4** (50 mg, 0.14 mmol), NEt_3 (39 μL, 0.28 mmol) and $[Ru(hmbz)Cl_2]_2$ (47 mg, 0.070 mmol) in MeOH (5 mL). The mixture was concentrated under reduced pressure, the resulting solid was washed with diethyl ether and petroleum ether. Recovery from the fritted glass funnel was performed by dissolution in dichloromethane followed by solvent evaporation, to afford *E*-**9** (85 mg, 0.13 mmol, 91% yield). Crystals suitable for X-Ray analysis were obtained by vapor diffusion of petroleum ether in an acetone solution of the complex. Black solid. M.p. *ca.* 280 °C. R_f 0.90 (CH_2Cl_2/MeOH: 9/1). ^{1}H-NMR (500 MHz, $(CD_3)_2CO$): 9.45 (dd, J = 7.5, 1.5 Hz, 1H), 8.05 (d, J = 8.5 Hz, 2H), 7.94 (dd, J = 8.0, 1.0 Hz, 1H), 7.82 (dd, J = 8.5, 1.0 Hz, 1H), 7.53–7.44 (m, 3H), 7.11 (td, J = 8.0, 1.0 Hz, 1H), 7.07 (d, J = 8.5 Hz, 2H), 6.64 (td, J = 8.5, 1.0 Hz, 1H), 2.66 (s, 3H), 2.23 (s, 3H), 1.82 (s, 18H). ^{13}C NMR (125 MHz, $(CD_3)_2CO$): 162.1, 161.0, 153.9, 152.5, 142.1, 133.6, 132.2, 132.0, 130.2 (2C), 129.2 (2C), 127.6, 121.5, 121.3, 119.6, 118.6, 97.0, 21.3, 19.1 (6C), 16.1 (6C), 1C missing. IR (ATR): 3873, 2602, 2498, 1591, 1567, 1473, 1452, 1384, 1328, 1304, 1288, 1248, 1211, 1159, 1140, 1084, 1037, 965, 942, 878, 854, 814, 780, 770, 750, 737, 708, 659. UV/Vis (MeOH): 484 (4300). HR-ESI-MS: 664.1294 ($C_{32}H_{37}ClN_3O_2RuS$, $[M+H]^+$; calc. 664.1341).

Ru(II) Complex *E*-**10**. Synthesized according to general procedure B using **5** (122 mg, 0.321 mmol), NEt_3 (90 μL, 0.68 mmol) and $[Ru(hmbz)Cl_2]_2$ (108 mg, 0.161 mmol) in MeOH (10 mL). The mixture was concentrated under reduced pressure, filtered and the solid washed with petroleum ether to afford *E*-**10** (212 mg, 0.313 mmol, 97% yield). Black solid. M.p. *ca.* 280 °C. R_f 0.90 (CH_2Cl_2/MeOH: 9/1). ^{1}H-NMR (400 MHz, CD_2Cl_2): 9.40 (d, J = 7.5 Hz, 1H), 7.93 (d, J = 8.5 Hz, 2H), 7.83 (dd, J = 8.5, 1.5 Hz, 1H), 7.73 (dd, J = 9.0, 1.0 Hz, 1H), 7.53–7.45 (m, 3H), 7.09–7.04 (m, 3H), 6.63 (td, J = 7.0, 1.0 Hz, 1H), 3.12 (m, 1H), 2.87 (m, 1H), 2.25 (s, 3H), 1.79 (s, 18H), 1.43 (t, J = 7.5 Hz, 3H). ^{13}C UDEFT NMR (100 MHz, CD_2Cl_2): 153.5, 150.7, 149.0, 142.3, 141.9, 139.6, 131.9, 131.6, 129.6, 129.3 (2C), 128.9 (2C), 127.2, 120.7, 120.6, 119.1, 118.3, 96.2 (6C), 25.7, 21.4, 16.1 (6C), 15.3. IR (ATR): 3873, 3059, 2960, 2603, 2497, 1590, 1568, 1473, 1453, 1397, 1384, 1326, 1300, 1283, 1246, 1204, 1168, 1137, 1084, 1036, 968, 941, 883, 851, 820, 790, 774, 749, 736, 708, 660. HR-ESI-MS: 678.1445 ($C_{33}H_{39}ClN_3O_2RuS$, $[M+H]^+$; calc. 678.1487).

Ru(II) Complex *E*-**11**. Synthesized according to general procedure B using **6** (133 mg, 0.338 mmol), NEt_3 (94 μL, 0.72 mmol) and $[Ru(hmbz)Cl_2]_2$ (113 mg, 0.169 mmol) in MeOH (10 mL). The mixture was concentrated under reduced pressure, filtered and the solid washed with petroleum ether to afford *E*-**11** (234 mg, in mixture with remaining traces of triethylammonium salt). Black solid. M.p. *ca.* 280 °C. R_f 0.85 (CH_2Cl_2/MeOH: 9/1). ^{1}H-NMR (400 MHz, $(CD_3)_2CO$): 9.53 (dd, J = 8.5, 1.0 Hz, 1H), 8.05 (d, J = 8.5 Hz, 2H), 7.83 (dd, J = 8.0, 1.0 Hz, 1H), 7.63 (dd, J = 7.5, 1.0 Hz, 1H), 7.56 (td, J = 7.5, 1.0 Hz, 1H), 7.49 (td, J = 8.5, 1.0 Hz, 1H), 7.17–7.10 (m, 2H), 7.07 (d, J = 8.5 Hz, 2H), 6.65 (dd, J = 7.5, 1.0 Hz, 1H), 3.64 (sept., J = 7.0 Hz, 1H), 2.23 (s, 3H), 1.83 (s, 18H), 1.47 (d, J = 7.0 Hz, 3H), 1.42 (d, J = 7.0 Hz, 3H). ^{13}C UDEFT NMR (100 MHz, $(CD_3)_2CO$): 160.3, 152.6, 149.9, 148.9, 146.2, 141.6, 132.6, 132.2, 130.3 (2C), 129.2 (2C), 127.5, 127.1, 121.6, 121.4, 119.6, 118.7, 97.0 (6C), 22.3 (2C), 21.2, 16.2 (6C), 1C missing. IR (ATR): 3873, 3060, 2974, 2602, 2497, 1590, 1567, 1473, 1452, 1397, 1382, 1327, 1299, 1285, 1245, 1209, 1193, 1158, 1139, 1098, 1086, 1035, 967, 940, 921, 851, 819, 774, 752, 739, 708, 661. HR-ESI-MS: 692.1602 ($C_{34}H_{41}ClN_3O_2RuS$, $[M+H]^+$; calc. 692.1648).

Ru(II) Complex *Z*-**12**. Synthesized according to general procedure B using **7** (89 mg, 0.24 mmol), NEt_3 (66 μL, 0.48 mmol) and $[Ru(hmbz)Cl_2]_2$ (67 mg, 0.12 mmol) in MeOH (8 mL). The mixture was concentrated under reduced pressure, filtered and the solid washed with a minimum amount of MeOH to afford *Z*-**12** (84 mg, 0.15 mmol, 62% yield). Crystals suitable for X-Ray analysis were obtained by vapor diffusion of petroleum ether in an acetone solution of the complex. Black solid. M.p. 247 °C. R_f 0.91 (CH_2Cl_2/MeOH: 95/5). ^{1}H-NMR (400 MHz, $(CD_3)_2CO$): 8.08 (d, J = 8.0 Hz, 2H), 7.74 (d, J = 8.5 Hz, 1H), 7.16 (d, J = 7.5 Hz, 1H), 7.10 (d, J = 8.0 Hz, 2H), 6.99–6.90 (m, 2H), 6.69 (d, J = 7.5 Hz, 1H), 6.25 (dd, J = 8.5, 1.0 Hz, 1H), 6.10 (td, J = 7.5, 1.0 Hz, 1H), 2.61 (s, 3H), 2.28 (s, 3H), 2.15 (s, 18H), 1.80 (s, 3H). ^{13}C NMR (100 MHz, $(CD_3)_2CO$): 154.7, 151.9, 149.1, 142.1, 140.0, 132.1, 131.7, 130.2 (3C), 129.5, 128.9 (2C), 127.9, 123.6, 121.9, 118.0, 117.0, 96.3 (6C), 21.3, 19.5, 19.1, 15.9 (6C). IR (ATR): 3507, 2914, 1588, 1559, 1460, 1383, 1309, 1301, 1284, 1248, 1217, 1136, 1100, 1085, 1028, 942, 908, 842, 822, 780, 762, 745, 735, 708, 659. UV/Vis (MeOH): 483 (4000). HR-ESI-MS: 678.1450 ($C_{33}H_{39}ClN_3O_2RuS$, $[M+H]^+$; calc. 678.1476).

Supplementary Material

Supporting Information for this article is available on the WWW under https://doi.org/10.1002/hlca.202300190.

Author Contribution Statement

J. L. performed synthetic work, photophysical experiments and computational studies; he analyzed the data and contributed to designing the experiments and writing the article. *P. R.* performed XRD experiments, analyzed the data and contributed to writing the article. *J. X.* contributed to the design of experiments and data analysis, and proofread the article. *N. B.* designed the experiments, analyzed the data and wrote the article.

Acknowledgements

This work was supported by a public grant overseen by the French National Research Agency (ANR) as part of the "Investissements d'Avenir" program (reference: ANR-11-LABX-0039, Labex CHARMMMAT) and was performed using HPC resources from the "Mésocentre" computing center of CentraleSupélec and École Normale Supérieure Paris-Saclay supported by CNRS and Région Île-de-France (http://mesocentre.centralesupelec.fr/).

Data Availability Statement

The data that support the findings of this study are available in the supplementary material of this article.

References

[1] O. Galangau, L. Norel, S. Rigaut, 'Metal complexes bearing photochromic ligands: photocontrol of functions and processes', *Dalton Trans.* **2021**, *50*, 17879–17891.

[2] S. Kaler, M. D. Jones, 'Recent advances in externally controlled ring-opening polymerisations', *Dalton Trans.* **2022**, *51*, 1241–1256.

[3] Z. Freixa, 'Photoswitchable catalysis using organometallic complexes', *Catal. Sci. Technol.* **2020**, *10*, 3122–3139.

[4] D. Gupta, A. K. Gaur, H. Kumar, S. Singh, S. Venkataramani, 'Light-Switchable Metal Complexes: Introducing Photoresponsive Behaviour Through Azoheteroarenes', *ChemPhotoChem* **2023**, e202300068.

[5] C.-C. Ko, V. W.-W. Yam, 'Coordination Compounds with Photochromic Ligands: Ready Tunability and Visible Light-Sensitized Photochromism', *Acc. Chem. Res.* **2018**, *51*, 149–159.

[6] D. Jago, E. E. Gaschk, G. A. Koutsantonis, 'History and fundamentals of molecular photochromism', *Aust. J. Chem.* **2023**, DOI 10.1071/CH23115.

[7] S. Panda, S. Dhara, A. Singh, S. Dey, G. Kumar Lahiri, 'Metal-coordinated azoaromatics: Strategies for sequential azo-reduction, isomerization and application potential', *Coord. Chem. Rev.* **2023**, *475*, 214895.

[8] K. Nakamura, M. Kondo, C. G. Krishnan, S. Takizawa, H. Sasai, 'Azopyridine-based chiral oxazolines with rare-earth metals for photoswitchable catalysis', *Chem. Commun.* **2021**, *57*, 7414–7417.

[9] J. L. Pratihar, P. Mandal, N. Sepay, D. Mal, T. Maity, C. K. Lai, P. Brandão, 'Spectroscopic characterization, structural investigation, DFT study, and Hirshfeld surface analysis of rhodium and ruthenium amido azo complexes', *J. Mol. Struct.* **2021**, *1241*, 130671.

[10] G. Vinoth, S. Indira, M. Bharathi, M. Sounthararajan, D. Sakthi, K. S. Bharathi, 'Appraisal of Ruthenium(II) complexes of (4-phenoxyphenylazo) ligands for the synthesis of primary amides by dint of hydroxylamine hydrochloride and aldehydes', *J. Organomet. Chem.* **2019**, *894*, 67–77.

[11] A. I. Uraev, K. A. Lyssenko, V. G. Vlasenko, Y. V. Zubavichus, M. P. Bubnov, N. I. Makarova, D. A. Garnovskii, A. S. Burlov, 'Synthesis, properties and structure of copper(II) complexes of quinolyl azo derivatives of pyrazole-5-one(thione)', *Polyhedron* **2018**, *146*, 1–11.

[12] K. G. Samper, S. C. Marker, P. Bayón, S. N. MacMillan, I. Keresztes, Ò. Palacios, J. J. Wilson, 'Reprint of "Anticancer activity of hydroxy- and sulfonamide-azobenzene platinum(II) complexes in cisplatin-resistant ovarian cancer cells"', *J. Inorg. Biochem.* **2017**, *177*, 335–343.

[13] A. I. Uraev, V. G. Vlasenko, A. S. Burlov, N. I. Makarova, K. A. Lyssenko, D. A. Garnovskii, 'Synthesis and structure of nickel and copper chelate complexes with coumarin azo ligand', *Mendeleev Commun.* **2018**, *28*, 205–207.

[14] K. Ghebreyessus, S. M. Cooper, 'Photoswitchable Arylazopyrazole-Based Ruthenium(II) Arene Complexes', *Organometallics* **2017**, *36*, 3360–3370.

[15] V. Sashuk, O. Danylyuk, 'A Thermo- and Photo-Switchable Ruthenium Initiator For Olefin Metathesis', *Chem. Eur. J.* **2016**, *22*, 6525–6531.

[16] R. I. Patia, K. Singh, D. L. Davies, F. Lelj, 'Photoisomerisation of Exo-Imine Complexes and the Role of MECP in the Reverse Thermal Equilibrium: An Experimental and DFT Computational Investigation.', *Chem. Eur. J.* **2023**, e202301570.

[17] C. Deo, N. Bogliotti, R. Métivier, P. Retailleau, J. Xie, 'Photoswitchable Arene Ruthenium Complexes Containing o-Sulfonamide Azobenzene Ligands', *Organometallics* **2015**, *34*, 5775–5784.

[18] C. Deo, H. Wang, N. Bogliotti, Y. Zang, P. Retailleau, X.-P. He, J. Li, J. Xie, 'Photoswitchable arene ruthenium and pentamethylcyclopentadienyl rhodium complexes containing o-sulfonamide azobenzene ligands: Synthesis, characterization and cytotoxicity', *J. Organomet. Chem.* **2016**, *820*, 111–119.

[19] C. Deo, N. Bogliotti, P. Retailleau, J. Xie, 'Triphenylphosphine Photorelease and Induction of Catalytic Activity from Ruthenium-Arene Complexes Bearing a Photoswitchable *o*-Tosylamide Azobenzene Ligand', *Organometallics* **2016**, *35*, 2694–2700.

[20] L. Rocard, J. Hannedouche, N. Bogliotti, 'Visible-Light-Initiated Palladium-Catalyzed Cross-coupling by PPh_3 Uncaging from an Azobenzene Ruthenium–Arene Complex', *Chem. Eur. J.* **2022**, *28*, e202200519.

[21] M. Reimann, E. Teichmann, S. Hecht, M. Kaupp, 'Solving the Azobenzene Entropy Puzzle: Direct Evidence for Multi-State Reactivity', *J. Phys. Chem. Lett.* **2022**, *13*, 10882–10888.

[22] S. Axelrod, E. Shakhnovich, R. Gómez-Bombarelli, 'Thermal Half-Lives of Azobenzene Derivatives: Virtual Screening Based on Intersystem Crossing Using a Machine Learning Potential', *ACS Cent. Sci.* **2023**, *9*, 166–176.

[23] D. Phapale, D. Das, 'Photoswitchable azobenzene functionalized anthraquinone and benzimidazole Ru(II)-p-cymene organometallic complexes', *J. Organomet. Chem.* **2020**, *913*, 121203.

[24] R. L. Martin, 'Natural transition orbitals', *J. Chem. Phys.* **2003**, *118*, 4775–4777.

[25] H. M. D. Bandara, S. C. Burdette, 'Photoisomerization in different classes of azobenzene', *Chem. Soc. Rev.* **2012**, *41*, 1809–1825.

[26] J. Long, L. Rocard, E. Van Elslande, P. Retailleau, J. Xie, N. Bogliotti, 'Light-Promoted Basic Nitrogen Unmasking in Arene Ruthenium Complexes Derived from *Z* -Configured 2,2′-Azobispyridine', *Chem. Eur. J.* **2023**, *29*, e202301301.

[27] The absolute configuration at the ruthenium center was determined following the modified Cahn-Ingold-Prelog priority rules discussed in E. B. Bauer, 'Chiral-at-metal complexes and their catalytic applications in organic synthesis', *Chem. Soc. Rev.* **2012**, *41*, 3153.

[28] C. F. Macrae, I. Sovago, S. J. Cottrell, P. T. A. Galek, P. McCabe, E. Pidcock, M. Platings, G. P. Shields, J. S. Stevens, M. Towler, P. A. Wood, '*Mercury 4.0*: from visualization to analysis, design and prediction', *J. Appl. Crystallogr.* **2020**, *53*, 226–235.

[29] J. J. McKinnon, D. Jayatilaka, M. A. Spackman, 'Towards quantitative analysis of intermolecular interactions with Hirshfeld surfaces', *Chem. Commun.* **2007**, 3814–3816.
[30] M. A. Spackman, D. Jayatilaka, 'Hirshfeld surface analysis', *CrystEngComm* **2009**, *11*, 19–32.
[31] P. R. Spackman, M. J. Turner, J. J. McKinnon, S. K. Wolff, D. J. Grimwood, D. Jayatilaka, M. A. Spackman, '*CrystalExplorer*: a program for Hirshfeld surface analysis, visualization and quantitative analysis of molecular crystals', *J. Appl. Crystallogr.* **2021**, *54*, 1006–1011.
[32] M. Piotto, M. Bourdonneau, K. Elbayed, J.-M. Wieruszeski, G. Lippens, 'New DEFT sequences for the acquisition of one-dimensional carbon NMR spectra of small unlabelled molecules', *Magn. Reson. Chem.* **2006**, *44*, 943–947.
[33] H. E. Gottlieb, V. Kotlyar, A. Nudelman, 'NMR Chemical Shifts of Common Laboratory Solvents as Trace Impurities', *J. Org. Chem.* **1997**, *62*, 7512–7515.
[34] G. R. Fulmer, A. J. M. Miller, N. H. Sherden, H. E. Gottlieb, A. Nudelman, B. M. Stoltz, J. E. Bercaw, K. I. Goldberg, 'NMR Chemical Shifts of Trace Impurities: Common Laboratory Solvents, Organics, and Gases in Deuterated Solvents Relevant to the Organometallic Chemist', *Organometallics* **2010**, *29*, 2176–2179.
[35] Gaussian 16, Revision B.01, M. J. Frisch, G. W. Trucks, H. B. Schlegel, G. E. Scuseria, M. A. Robb, J. R. Cheeseman, G. Scalmani, V. Barone, G. A. Petersson, H. Nakatsuji, X. Li, M. Caricato, A. V. Marenich, J. Bloino, B. G. Janesko, R. Gomperts, B. Mennucci, H. P. Hratchian, J. V. Ortiz, A. F. Izmaylov, J. L. Sonnenberg, Williams, F. Ding, F. Lipparini, F. Egidi, J. Goings, B. Peng, A. Petrone, T. Henderson, D. Ranasinghe, V. G. Zakrzewski, J. Gao, N. Rega, G. Zheng, W. Liang, M. Hada, M. Ehara, K. Toyota, R. Fukuda, J. Hasegawa, M. Ishida, T. Nakajima, Y. Honda, O. Kitao, H. Nakai, T. Vreven, K. Throssell, J. A. Montgomery Jr., J. E. Peralta, F. Ogliaro, M. J. Bearpark, J. J. Heyd, E. N. Brothers, K. N. Kudin, V. N. Staroverov, T. A. Keith, R. Kobayashi, J. Normand, K. Raghavachari, A. P. Rendell, J. C. Burant, S. S. Iyengar, J. Tomasi, M. Cossi, J. M. Millam, M. Klene, C. Adamo, R. Cammi, J. W. Ochterski, R. L. Martin, K. Morokuma, O. Farkas, J. B. Foresman, D. J. Fox, Gaussian, Inc., Wallingford CT, **2016**.
[36] M. D. Hanwell, D. E. Curtis, D. C. Lonie, T. Vandermeersch, E. Zurek, G. R. Hutchison, *J. Cheminf.* **2012**, *4*, 1–17.
[37] D. Rivillo, H. Gulyás, J. Benet-Buchholz, E. C. Escudero-Adán, Z. Freixa, P. W. N. M. van Leeuwen, 'Catalysis by Design: Wide-Bite-Angle Diphosphines by Assembly of Ditopic Ligands for Selective Rhodium-Catalyzed Hydroformylation', *Angew. Chem. Int. Ed.* **2007**, *46*, 7247–7250.

Received October 24, 2023
Accepted November 30, 2023

